RSC Advances

PAPER

View Article Online
View Journal | View Issue

Cite this: *RSC Adv.*, 2016, **6**, 47864

# Organophosphorous surfactant-assistant synthesis of SAPO-34 molecular sieve with special morphology and improved MTO performance†

Chan Wang,[abc] Miao Yang,[ab] Wenna Zhang,[abc] Xiong Su,[abc] Shutao Xu,[ab] Peng Tian*[ab] and Zhongmin Liu*[ab]

Received 10th March 2016
Accepted 6th May 2016

DOI: 10.1039/c6ra06428k

www.rsc.org/advances

With the aid of self-designed organophosphorous surfactant [2-(diethoxylphosphono)propyl] hexadecyldimethylammonium bromide (DPHAB), SAPO-34s with various special morphologies have been hydrothermally synthesized by using tetraethylammonium hydroxide (TEAOH), diethylamine (DEA) and triethylamine (TEA) as templates, respectively. The synthesized SAPO-34s were well characterized by XRD, XRF, SEM, $N_2$ adsorption–desorption, solid state NMR and $NH_3$-TPD measurements. The status of DPHAB was also investigated by using FT-IR, $^{13}C$ NMR, TG–DTA and $^{31}P$ NMR measurements as well as density functional theory calculations. It is found that the addition of DPHAB changes the crystal morphology dramatically and the aggregation degree of the crystals increases with the rising DPHAB/$H_3PO_4$ ratio. Moreover, microporous templates play an important role in the synthesis of mesoporous SAPO-34. TEAOH, which has the strongest interaction energy with the CHA framework among the investigated templates, shows the best cooperating ability with an organophosphorous surfactant to direct the formation of nanosized and mesoporous SAPO-34. The prepared SAPO-34s showed improved catalytic properties in the methanol-to-olefins (MTO) reaction.

## 1 Introduction

Silicoaluminophosphate molecular sieves, as an important class of crystalline microporous materials, have been widely used as heterogeneous acid catalysts due to their uniform microporous structure, medium/strong acidity and excellent thermal and hydrothermal stabilities.[1] Especially, small-pore SAPO-34 molecular sieves exhibit excellent performance in the methanol-to-olefins (MTO) reaction,[2–4] based on which some commercial scale MTO plants have been successfully started up.[5] In spite of this, the SAPO-34 catalyst suffers from rapid deactivation due to the fast coke formation and mass transport limitation caused by its small pore and large cavity structure. So, the fluidized-bed reaction technique with continuous regenerating and recycling has to be applied in the industrial MTO process.[6] Improving the SAPO-34 catalyst would be of great significance from the scientific and practical points of view.

Considerable efforts have been made to optimize the SAPO-34 catalyst,[7–11] and the product morphology control is considered as an attractive solution to relieve the diffusion resistance. Up to now, various strategies including modifying heating modes,[12–15] adding additives,[16–20] changing raw materials[8] and synthetic routes[11] have been tried to change the morphology of the SAPO-34 molecular sieve. Some SAPO-34s with smaller crystal size and hierarchical porous structure have shown better catalytic performance for the MTO reaction. Recently, we have also synthesized a spherical SAPO-34 nanosheet assembly by using [3-(trimethoxysilyl)propyl]octadecyldimethylammonium chloride (TPOAC) as the mesoporogen and a part of silica source, and diethylamine (DEA) as the microporous template.[21] Meanwhile, the hierarchical SAPO-34s have also been synthesized by others with TPOAC mesoporogen together with other microporous templates.[17,22] Although the synthesis method is similar, the synthesized SAPO-34s displayed remarkably different morphologies and MTO catalytic activity. It is thus believed that microporous template plays an important role in the crystallization of SAPO-34 which results in significantly different SAPO-34 morphologies and acidity.

Organosilane surfactant has been proved to be an effective mesoporogen and silica source to synthesize hierarchical SAPO-34. The existence of multifunctional groups in the designed surfactant can effectively inhibit the phase separation of microporous and mesoporous structures. At the same time, it plays as a special silica source which would affect the acidity of

[a]*Dalian National Laboratory for Clean Energy, Dalian Institute of Chemical Physics, Chinese Academy of Sciences, Dalian, P. R. China. E-mail: tianpeng@dicp.ac.cn; liuzm@dicp.ac.cn*

[b]*National Engineering Laboratory for Methanol to Olefins, Dalian Institute of Chemical Physics, Chinese Academy of Sciences, Dalian, P. R. China*

[c]*University of Chinese Academy of Sciences, Beijing, P. R. China*

† Electronic supplementary information (ESI) available. See DOI: 10.1039/c6ra06428k

the SAPO-34 product. To explore more effective method to tune the SAPO crystal morphology, organophosphorous surfactant seems to be an interesting choice. The incorporation of P from organophosphorous surfactant into the framework will not change the acidity of SAPO framework, which allows an easier control of the product acidity. As we know, several organic phosphorus compounds have been used to synthesize molecular sieve materials. By using tetrabutylphosphonium as the only structure-directing agent (SDA), Tsapatsis *et al.* synthesized a self-pillared MFI zeolite composed of single unit cell lamella (2 nm thick).[23] The SDA creates an environment to encourage the repetitive branching process which results in a "house-of-cards" arrangement of the zeolite nanosheets with 2 to 7 nm mesopores. These results suggest that organophosphorous compound could play an important role in the synthesis of molecular sieve with special structure and morphology. However, report on the synthesis of SAPO molecular sieves with the aid of organophosphorous compound is rare.[24]

In the present work, a new organophosphorous surfactant containing a hydrolysable diethoxylphosphono part, a quaternary ammonium group and a hydrophobic alkyl-chain tail was designed, synthesized and used to synthesize SAPO-34 together with different microporous templates, including tetraethylammonium hydroxide (TEAOH), diethylamine (DEA) and triethylamine (TEA). The prepared SAPO-34s were well characterized, which showed different morphologies depending on the different microporous templates used and the DPHAB/$H_3PO_4$ ratio. The status of the organophosphorous molecule was investigated by various characterizations together with the density functional theory calculation. The MTO catalytic performances of the synthesized SAPO-34s were evaluated.

# 2 Experimental section

## 2.1 Materials

Orthophosphoric acid ($H_3PO_4$, 85 wt%), tetraethyl orthosilicate (TEOS, 98 wt%), aluminium isopropoxide ($Al(i\text{-}C_3H_7O)_3$, 99 wt%), tetraethylammoniumhydroxide (TEAOH, 25 wt%), diethylamine (DEA, 99 wt%) and triethylamine (TEA, 99 wt%) were purchased from Tianjin Kemiou Chemical Reagent Co. Triethyl phosphite (98 wt%), 1,3-dibromopropane (99 wt%) and *N*,*N*-dimethylhexadecylamine (99 wt%) were purchased from Aladdin Chemical Inc. All chemicals were used as received without further purification.

## 2.2 Synthesis of [2-(diethoxylphosphono)propyl] hexadecyldimethylammonium bromide ([$(C_2H_5O)_2P(O)$–$C_3H_6$–$N(CH_3)_2$–$C_{16}H_{33}$]Br)

The organophosphorous surfactant [2-(diethoxylphosphono) propyl]hexadecyldimethylammonium bromide was prepared by a two-step reaction according to Scheme S1.† Firstly, $(C_2H_5O)_2P(O)$–$C_3H_6Br$ as an intermediate product was synthesized by refluxing of 36.92 g (1.11 mol) triethyl phosphite and 224.33 g (5.55 mol) 1,3-dibromopropane at 165 °C for 1 h under a nitrogen stream. After cooling to room temperature and evaporating the unreacted reactants, the colorless liquid product was obtained (yield: 86%). $^1$H NMR ($CDCl_3$): $\delta$ 1.14 (6H, $CH_3$, m), 1.72 (2H, $CH_2\underline{CH_2}CH_2$, m), 1.96 (2H, $CH_2P$, t, $J$ 6.2 Hz), 3.30 (2H, $BrCH_2$, t, $J$ 6.4 Hz), 3.91 (4H, $OCH_2$, m). $^{13}$C NMR ($CDCl_3$): $\delta$ 16.15 ($CH_3$, d, $J$ 4.6 Hz), 23.38 ($CH_2\underline{CH_2}CH_2$, s), 25.69 ($CH_2P$, d, $J$ 16 Hz), 33.27 ($BrCH_2$, m), 61.30 ($OCH_2$, d, $J$ 20 Hz). $^{31}$P NMR ($CDCl_3$): $\delta$ 31.8. Secondly, 53.28 g (0.21 mol) $(C_2H_5O)_2P(O)$–$C_3H_6Br$ and 56.75 g (0.21 mol) *N*,*N*-dimethylhexadecylamine were stirred with 1.77 g (0.01 mol) KI catalyst in 55.38 g (1.2 mol) ethyl alcohol. The mixture was refluxed at 80 °C for 40 h under a nitrogen stream. After cooling to room temperature and evaporating solvent, a light yellow thick liquid remained. The residual liquid was then purified by recrystallization to obtain the product [$(C_2H_5O)_2P(O)$–$C_3H_6$–$N(CH_3)_2$–$C_{16}H_{33}$]Br (denoted as DPHAB, yield: 83%). $^1$H NMR ($CDCl_3$): $\delta$ 0.80 (3H, $CH_3$ in $C_{16}H_{33}$, t), 1.17 (26H, $CH_2$ in $C_{16}H_{33}$, m), 1.26 (6H, $CH_3$ in $OC_2H_5$, t), 1.6–2.3 (6H, $CH_2$ in $PC_3H_6N$ and $C_{16}H_{33}$, m), 3.33 (6H, $CH_3N$, s), 3.42 (2H, $CH_2$ in $C_{16}H_{33}$, t, 8 Hz), 3.71 (2H, $CH_2$ in $PC_3H_6N$, m), 4.03 (4H, $CH_2$ in $OC_2H_5$, m). $^{13}$C NMR ($CDCl_3$): $\delta$ 13.9 ($CH_3$ in $C_{16}H_{33}$, s), 16.30 ($CH_3$ in $OC_2H_5$, m), 20.97 ($CH_2$ in $PC_3H_6N$, s), 22.46 ($CH_2$ in $PC_3H_6N$ and $C_{16}H_{33}$, m), 26.08 ($CH_2$ in $C_{16}H_{33}$, s), 29.0–29.5 ($CH_2$ in $C_{16}H_{33}$, m), 31.70 ($CH_2$ in $C_{16}H_{33}$, s), 51.05 ($CH_3N$, s), 61.90 ($CH_2$ in $C_{16}H_{33}$, s), 62.80 ($CH_2$ in $PC_3H_6N$, m), 64.11 ($CH_2$ in $OC_2H_5$, s). $^{31}$P NMR ($CDCl_3$): $\delta$ 30.7. Little intermediate product remained in the final product. The purity of the intermediate and final products was confirmed by $^1$H, $^{13}$C and $^{31}$P NMR analyses, and the spectra are shown in Fig. S1.†

## 2.3 Synthesis of SAPO-34s

A typical synthesis procedure was as follows. A certain amount of DPHAB was firstly added into deionized water and stirred for 2 h. Then, desired amount of aluminium isopropoxide, organic amine, tetraethyl orthosilicate and phosphoric acid were added in sequence. After further stirring for 2–5 h, the obtained gel was transferred into a stainless steel autoclave and heated statically at 200 °C for a certain time under autogenous pressure. The products were recovered by filtration, washed with deionized water and dried in air. The molar composition of the gel is $(2.0\text{–}3.0)R : (1.0\text{–}1.2)P_2O_5 : 1.0Al_2O_3 : 0.5SiO_2 : 150H_2O$, where R is the microporous template, and $P_2O_5$ is the mixture of DPHAB and $H_3PO_4$. The molar ratio of DPHAB/$H_3PO_4$ changes from 0 to $\infty$. The products are denoted as S-R-*n*, where R and *n* refer to the microporous template and the molar ratio of DPHAB/$H_3PO_4$ in the gel, respectively. For comparison, conventional SAPO-34s were prepared by using the corresponding template but without any DPHAB. The detailed synthesis and characterization information are provided in the ESI.†

The yields of products were calculated by the following equation:

$$\text{Yield} = (M_{\text{sample}} \times 75\%)/M(Al_2O_3 + P_2O_5 + SiO_2)_{\text{gel}} \times 100\%,$$

where $M_{\text{sample}}$ and $M(Al_2O_3 + P_2O_5 + SiO_2)_{\text{gel}}$ stand for the weight of the products and the dry mass of inorganic oxides in the starting mixture, respectively. 75% is the estimated average value of framework compounds included in the samples.

### 2.4 Characterization

The powder XRD pattern was recorded on a PANalytical X' 50 Pert PRO X-ray diffractometer with Cu-Kα radiation ($\lambda = 1.54059$ Å), operating at 40 kV and 40 mA. The chemical composition of the samples was determined with Philips Magix-601 X-ray fluorescence (XRF) spectrometer. The crystal morphology was observed by scanning electron microscopy (SEM) using a TM3000 (Hitachi) and field emission SEM (Hitachi SU8020). Textural properties of the calcined samples were determined by $N_2$ adsorption–desorption at 77 K on a Micromeritics ASAP 2020 system. The total surface area was calculated based on the BET equation. The micropore volume, micropore surface area and external surface area were evaluated using the *t*-plot method. Mesopore volume was evaluated from the adsorption isotherm by Barrett–Joyner–Halenda (BJH) method. The temperature-programmed desorption of ammonia ($NH_3$-TPD) was carried out with an Autochem II 2920 equipment (Micromeritics). 0.2 grams of the sample particles (40–60 mesh) were loaded into a U-quartz tube and pretreated at 650 °C for 60 min under He flow. After cooling down to 100 °C, a gas mixture of $NH_3$ and He flow was introduced to saturate the sample surface with $NH_3$ adsorption (60 min). After this, He flow was purged through the sample for 30 min to remove the weakly adsorbed $NH_3$ molecules. The measurement of the desorbed $NH_3$ was performed from 100 to 650 °C (10 °C $min^{-1}$) under He flow (20 ml $min^{-1}$). The liquid nuclear magnetic resonance (NMR) spectra were recorded on a Bruker Avance III 400 MHz NMR spectrometer. $CDCl_3$ and $D_2O$ were used as the solvent in the measurement of $^1H$, $^{13}C$ and $^{31}P$ NMR of DPHAB, and $^{31}P$ NMR of mother liquid after crystallization, respectively. Tetramethylsilane ($\delta = 0$ ppm) or $CDCl_3$ ($\delta = 7.27$ ppm) serve as the internal standard for $^1H$ NMR, and $CDCl_3$ (77.16 ppm) for $^{13}C$ NMR. All the solid state NMR experiments were performed on a Bruker Avance III 600 spectrometer equipped with a 14.1 T wide-bore magnet. The resonance frequencies were 150.9, 242.9, 156.4 and 119.2 MHz for $^{13}C$, $^{31}P$, $^{27}Al$ and $^{29}Si$, respectively. $^{13}C$, $^{31}P$ and $^{27}Al$ MAS NMR experiments were performed on a 4 mm MAS probe with a spinning rate of 12 kHz. $^{29}Si$ MAS NMR spectrum was recorded with a 7 mm MAS probe with a spinning rate of 6 kHz. Chemical shifts were referenced to adamantane for $^{13}C$, 85% $H_3PO_4$ for $^{31}P$, $(NH_4)Al(SO_4)_2 \cdot 2H_2O$ for $^{27}Al$ and 4,4-dimethyl-4-silapentane sulfonate sodium salt (DSS) for $^{29}Si$. Thermogravimetric and differential thermal analysis (TG and DTA) were performed on a TA SDTQ600 analyzer with the temperature-programmed rate of 10 °C $min^{-1}$ in air. The Fourier transformed infrared (FT-IR) spectra were carried out on a Bruker Tensor 27 instrument with a resolution of 4 $cm^{-1}$. The pallets were made by mixing the KBr and samples quantitatively.

### 2.5 Calculations

Templating ability to the formation of SAPO-34 was evaluated by the interaction energy between template–zeolite in CHA structure.[25–27] The energy was obtained by molecular modeling. The locator and maximum loading of templates were performed using Monte Carlo-simulated annealing in adsorption locator code.[28,29] The organic templates structure and the interaction energies between the template and CHA structure were described with the COMPASS force field using the Forcite code. The COMPASS force field has been applied widely on the study of interaction between zeolite framework and organic molecule.[29,30] The unit cell and the positions of framework atoms were fixed in the optimization progress. The interaction energy $E_{inter}$ was calculated as: $E_{inter} = E - E_{zeolite} - E_{template}$, where $E$, $E_{zeolite}$, $E_{template}$ refer to calculation energies of the system, *i.e.*, template inside CHA structure, CHA framework and organic amine template, respectively. All the calculations were performed in Material Studio software.

Density functional theory (DFT) calculation is a useful tool to understand molecular properties and describe the atoms behavior in the molecule.[31–33] It was used herein to investigate the reactivity and the stability of the DPHAB molecule. Geometry optimization of organophosphorous surfactant was performed at the DFT B3LYP level theory using a 6-31G* basis set with Gaussian 09 program. Molecular electrostatic potential (MEP) was determined at the same level of theory B3LYP/6-31G* with the optimized structure.

### 2.6 Catalytic tests

Methanol to olefins (MTO) reaction was performed in a quartz tubular fixed-bed reactor at atmospheric pressure. 0.3 g calcined catalyst (40–60 mesh) was loaded in the quartz reactor and activated at 550 °C in a He flow of 30 ml $min^{-1}$ for 1 h before starting each reaction run, and then the temperature was adjusted to a reaction temperature of 450 °C. The methanol was fed by passing the carrier gas (42 ml $min^{-1}$) through a saturator containing methanol at 30 °C, which gave a weight hourly space velocity (WHSV) of 3 $h^{-1}$. The reaction products were analyzed using an online gas chromatograph (Agilent GC 7890N), equipped with a flame ionization detector (FID) and Plot-Q column.

## 3 Results and discussion

### 3.1 Synthesis and characterization of SAPO-34 molecular sieve

SAPO-34s were synthesized by using DPHAB together with different microporous templates including TEAOH, DEA and TEA. The results are shown in Table 1 and Fig. S2–S4.† When TEAOH is used, pure SAPO-34 was readily synthesized in the DPHAB/$H_3PO_4$ ratio range of 0 to 1/2. Dense phase is the final product when DPHAB is used as the only phosphor source. When DEA or TEA is used instead, pure SAPO-34 can only be obtained with the DPHAB/$H_3PO_4$ smaller than 1/5. Larger amount of DPHAB leads to impurity or amorphous phase. It is also noted that the addition of DPHAB slows down the crystallization rate. Conventional SAPO-34 (S-TEAOH-0) can be well crystallized within 3 days. When DPHAB is introduced, the reaction takes 6, 5 and 10 days for TEAOH, DEA and TEA system, respectively. The yields of the three systems are similar and decrease as the increasing DPHAB/$H_3PO_4$ ratio. It is deduced that DPHAB is not as active as $H_3PO_4$, therefore, the increased DPHAB/$H_3PO_4$ ratio results in a deficiency of effective

 

Table 1 Reaction conditions[a] and results of SAPO molecular sieve synthesized with DPHAB

| Sample | DPHAB/$H_3PO_4$ | Product | Crystallization time/days | Product yield | Product composition |
|---|---|---|---|---|---|
| S-TEAOH-0[b] | 0 | SAPO-34 | 3 | 47.3% | $Al_{0.498}P_{0.390}Si_{0.112}O_2$ |
| S-TEAOH-1/9 | 1/9 | SAPO-34 | 6 | 74.6% | $Al_{0.488}P_{0.394}Si_{0.118}O_2$ |
| S-TEAOH-1/6 | 1/6 | SAPO-34 | 6 | 65.3% | $Al_{0.468}P_{0.419}Si_{0.113}O_2$ |
| S-TEAOH-1/2 | 1/2 | SAPO-34 | 6 | 49.3% | $Al_{0.490}P_{0.393}Si_{0.117}O_2$ |
| S-TEAOH-∞ | ∞ | Dense phase | 6 | — | $Al_{0.411}P_{0.506}Si_{0.083}O_2$ |
| S-DEA-1/6 | 1/6 | SAPO-34 | 5 | 52.3% | $Al_{0.487}P_{0.392}Si_{0.117}O_2$ |
| S-DEA-1/5 | 1/5 | SAPO-34 | 5 | 49.6% | $Al_{0.487}P_{0.406}Si_{0.107}O_2$ |
| S-DEA-1/3 | 1/3 | SAPO-34 + lamellar phase | 5 | 39.6% | — |
| S-DEA-1/2 | 1/2 | Amorphous | 5 | — | — |
| S-TEA-1/6 | 1/6 | SAPO-34 | 10 | 62.5% | $Al_{0.487}P_{0.404}Si_{0.109}O_2$ |
| S-TEA-1/5 | 1/5 | SAPO-34 | 10 | 60.3% | $Al_{0.489}P_{0.410}Si_{0.101}O_2$ |
| S-TEA-1/3 | 1/3 | Amorphous | 10 | — | — |

[a] The initial gel molar composition are $Al_2O_3/P_2O_5/SiO_2/TEAOH/H_2O = 1.0/1.2/0.5/2.0/150$, $Al_2O_3/P_2O_5/SiO_2/DEA/H_2O = 1.0/1.0/0.5/2.0/150$ and $Al_2O_3/P_2O_5/SiO_2/TEA/H_2O = 1.0/1.0/0.5/3.0/150$. [b] The estimated value of framework compounds is 85% used for the yield calculation.

phosphorus source and a reduced yield. The Si contents of the obtained products are comparable although they were synthesized with different template and DPHAB/$H_3PO_4$ ratio. Comparing the three synthetic systems, TEAOH leads to the widest crystallization region and the relatively short crystallization time. It is speculated that TEAOH has better templating ability. The templating abilities of the three templates for the formation of SAPO-34 were evaluated by comparing the interaction energy ($E_{inter}$) between template and the CHA framework, and the $E_{inter}$ were obtained by the molecular modeling and calculation. The modeled positions of the three templates in the CHA structure are shown in Fig. S5.† The calculated $E_{inter}$ for TEAOH, DEA and TEA are −79.70, −41.88 and −24.30 kcal $mol^{-1}$, respectively, which give the order of $E_{TEAOH} < E_{DEA} < E_{TEA}$. The result indicates that TEAOH has the best templating ability within the three structure directing agents.

The morphologies of the SAPO-34s synthesized with TEAOH are presented in Fig. 1. Without DPHAB, the S-TEAOH-0 presents typical rhombohedral crystals with the particle size of *ca.* 2 μm (Fig. 1a and b). Upon addition of DPHAB, the primary particle size of SAPO-34 product decreases to *ca.* 50–500 nm, which aggregate in different degree (Fig. 1c–h). Interestingly, the aggregation degree of nanocrystalline raises with the increased DPHAB. When the DPHAB/$H_3PO_4$ ratio reaches to 1/2, the SAPO-34 product becomes regular 5–10 μm sphere which is consisted of SAPO-34 slices, and the thickness of the SAPO-34 slice is 50–100 nm (inset of Fig. 1h). The crystal morphologies of SAPO-34s synthesized with DEA and TEA templates were also examined by SEM. As seen in Fig. 2, S-DEA-1/6 presents a worm-like morphology with a crystal size of around 2 μm (Fig. 2a); while S-DEA-1/5 presents a spherical morphology with a rough surface and relatively large crystal size of around 30 μm (Fig. 2b), which are quite different from the conventional rhombohedral morphology (Fig. S6†). Similarly, S-TEA-1/6 and S-TEA-1/5 exhibit the dispersed pyramidal morphology (*ca.* 5 μm) and a spherical aggregation (*ca.* 25 μm), respectively (Fig. 2c and d). The type of template and minor variation of DPHAB can trigger obvious changes for the morphology of SAPO-34. It indicates that both the type of template and DPHAB have significant impact on the crystallization of SAPO-34. The combined use of TEAOH and DPHAB leads to the smallest primary (50–500 nm) and secondary (5–10 μm) particles, which suggests that the TEAOH template may favor more SAPO-34 nucleation. The crystal morphology change and aggregation should be related to the addition of DPHAB. Surfactants have

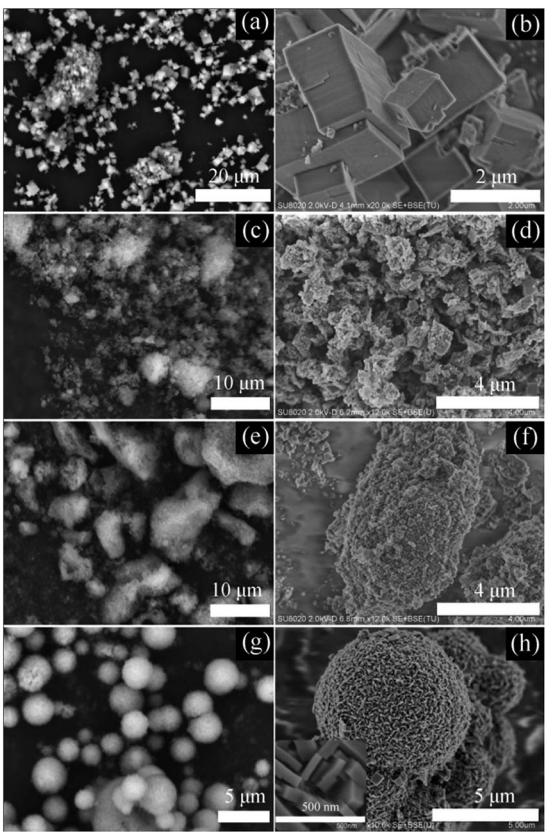


Fig. 1 SEM images of as-synthesized samples prepared with TEAOH and different DPHAB/$H_3PO_4$: S-TEAOH-0 (a and b), S-TEAOH-1/9 (c and d), S-TEAOH-1/6 (e and f) and S-TEAOH-1/2 (g and h).

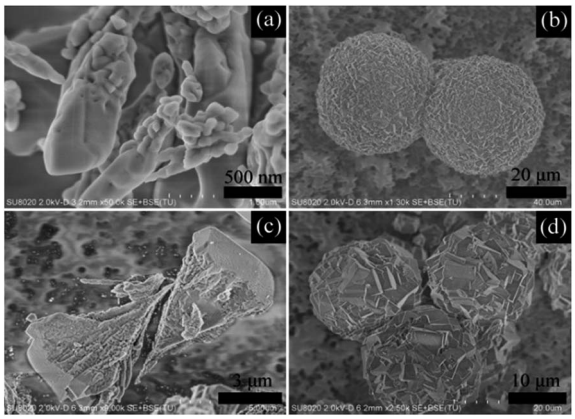


Fig. 2 SEM images of as-synthesized samples prepared with DEA/TEA and different DPHAB/$H_3PO_4$: S-DEA-1/6 (a), S-DEA-1/5 (b), S-TEA-1/6 (c) and S-TEA-1/5 (d).

been widely used to control the morphology of various materials due to their efficient self-assembly properties.[34–37] In our previous work, a spherical self-assembly of SAPO-34 nanosheets was achieved by using TPOAC as a mesogorogen.[21] The surfactant is a very potent surface stabilizer, which can lower the energy cost for creating new surfaces, thus affecting crystal splitting and changing the morphologies of the crystal. In our current work, DPHAB plays a similar role as TPOAC which leads to the self-assembly of SAPO-34 primary crystals to reduce the product surface energy.

The $N_2$ adsorption–desorption isotherms of SAPO-34 samples are given in Fig. 3 and S7.† All the samples have type I isotherms typical for pure microporous material except for S-TEAOH-1/2. S-TEAOH-1/2 shows combined features of type I and IV isotherms with two steep steps in the $P/P_0 < 0.01$ and $0.40 < P/P_0 < 0.90$ regions, corresponding to filling of the micropore volumes and capillary condensation in the mesopores, respectively. Correspondingly, the mesopore size distribution of S-TEAOH-1/2 is centered at 5.6 nm, as shown in the inset of Fig. 3. The textural properties of the samples are given in Table 2. S-TEAOH-1/2 exhibits the largest BET surface area

Table 2 Textural properties of the SAPO-34 samples

| Sample | $S_{BET}$[a] ($m^2\ g^{-1}$) | $S_{mic}$[b] ($m^2\ g^{-1}$) | $S_{Ext}$[c] ($m^2\ g^{-1}$) | $V_{mic}$[d] ($cm^3\ g^{-1}$) | $V_{meso}$[e] ($cm^3\ g^{-1}$) |
|---|---|---|---|---|---|
| S-TEAOH-0 | 602 | 593 | 9 | 0.28 | 0.02 |
| S-TEAOH-1/9 | 613 | 583 | 30 | 0.27 | 0.09 |
| S-TEAOH-1/2 | 673 | 577 | 96 | 0.27 | 0.18 |
| S-DEA-1/6 | 631 | 608 | 23 | 0.28 | 0.10 |
| S-DEA-1/5 | 622 | 597 | 25 | 0.28 | 0.02 |
| S-TEA-1/6 | 591 | 573 | 18 | 0.27 | 0.07 |
| S-TEA-1/5 | 587 | 575 | 12 | 0.27 | 0.02 |

[a] BET surface area. [b] *t*-Plot micropore surface area. [c] *t*-Plot external surface area. [d] *t*-Plot micropore volume. [e] BJH adsorption volume.

($673\ m^2\ g^{-1}$) and external surface area ($96\ m^2\ g^{-1}$) owing to the high crystallinity and the presence of intercrystal mesopores. The other samples also exhibit high BET surface area and large micropore volume indicating their good crystallinity.

Solid-state $^{31}P$, $^{27}Al$ and $^{29}Si$ NMR characterization were measured for the as-synthesized samples S-TEAOH-1/2, S-DEA-1/6 and S-TEA-1/6. The $^{31}P$ NMR spectra are shown in Fig. 4, and the corresponding $^{27}Al$ and $^{29}Si$ NMR spectra are given in Fig. S8.† All the $^{31}P$ NMR spectra give only strong resonance peak at around −29 ppm suggesting the predominant tetrahedral $PO_4$ environment in the framework for the three samples.[38] The missing of signal at around 30.7 ppm indicates that the samples do not include any organic phosphorous species. The $^{27}Al$ NMR spectra (Fig. S8A†) give a strong resonance at 39 ppm arising from tetrahedral Al species, and another weak signal at 10 ppm attributed to penta-coordinated Al formed by additional interactions of water or template molecule with the framework aluminum.[39] Regarding to the $^{29}Si$ NMR spectra (Fig. S8B†), all the three samples have a apparent resonance at −91 ppm ascribed to Si(4Al) species.[40] The presence of signal at around −96 ppm is ascribed to the environment of Si(3Al).[40] For sample S-TEAOH-1/2, more remarkable peaks emerge at around −101, −105 and −110 ppm corresponding to Si(2Al), Si(1Al) and Si-island, respectively.[40] The presence of Si($n$Al) ($n$ = 0–2)

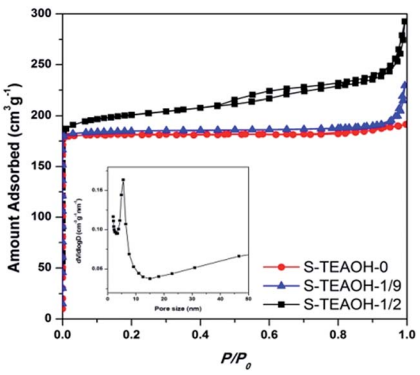


Fig. 3 Nitrogen adsorption/desorption isotherms of calcined S-TEAOH-0, S-TEAOH-1/9 and S-TEAOH-1/2, and BJH pore size distribution of calcined S-TEAOH-1/2 (inset).

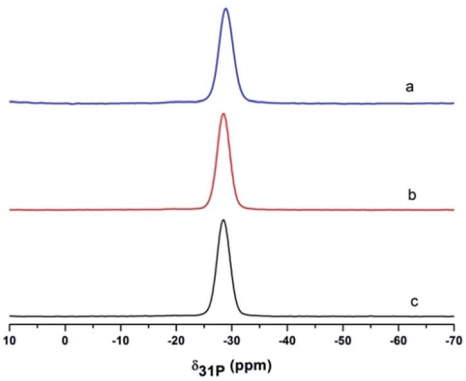


Fig. 4 $^{31}P$ NMR spectra of as-synthesized S-TEAOH-1/2 (a), S-DEA-1/6 (b) and S-TEA-1/6 (c).

species may be caused by the larger external surface of S-TEAOH-1/2.

### 3.2 Status of DPHAB

The above characterizations clearly demonstrate that the introduction of DPHAB has a significant impact on the crystallization and morphology of SAPO-34, but the organic phosphorous species may be not involved in the SAPO-34 products. So it is necessary to investigate the status of DPHAB in the reaction. FT-IR was used to check the organic species in the product. As seen in Fig. 5, both S-TEAOH-0 and S-TEAOH-1/2 exhibit bands at 2927 and 2850 $cm^{-1}$ assigned to the characteristic stretching vibration of C–H groups.[24] Obviously, the bands for S-TEAOH-1/2 are much stronger than that of S-TEAOH-0, which suggests that more organic species are included in S-TEAOH-1/2. In contrast, the FT-IR spectra of S-DEA-1/6 and S-TEA-1/6 are similar to their corresponding conventional samples (Fig. S9†). It indicates that there is not any additional organic species involved in the two samples except the microporous template.

In order to reveal the involved organic species in sample S-TEAOH-1/2, $^{13}C$ MAS NMR was further measured, and the spectrum is given in Fig. 6. Two signals at 51.8 and 6.4 ppm can be attributed to $-CH_2$ and $-CH_3$ groups of TEAOH template, and

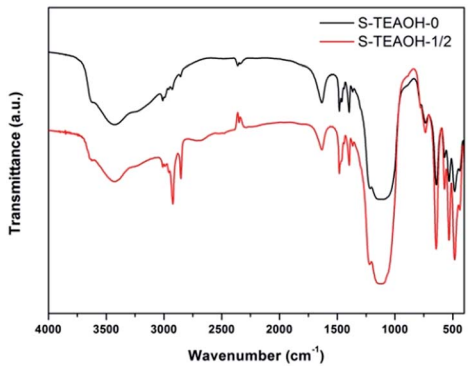


Fig. 5 FT-IR spectra of as-synthesized S-TEAOH-0 and S-TEAOH-1/2.

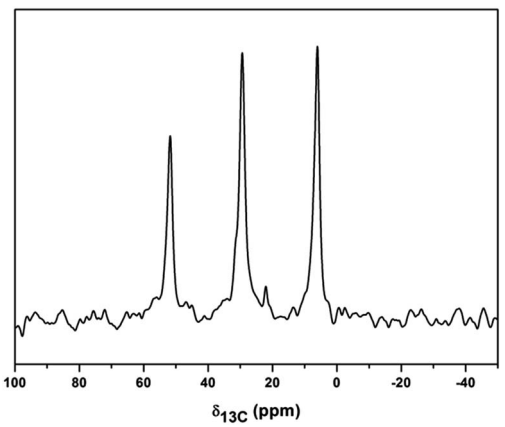


Fig. 6 $^{13}C$ MAS NMR spectrum of as-synthesized S-TEAOH-1/2.

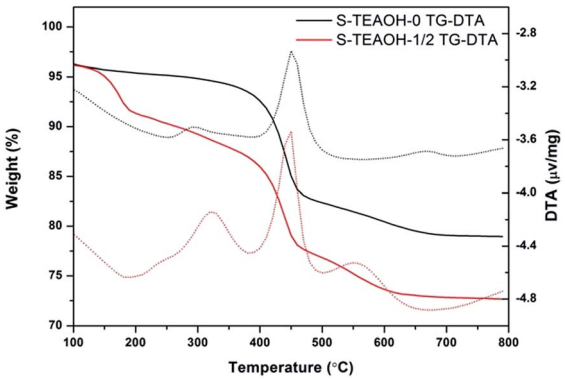


Fig. 7 TG–DTA curves of as-synthesized S-TEAOH-0 and S-TEAOH-1/2.

the strong signal at 29.5 ppm is assigned to methylene moieties which should come from the long-alkyl chain of DPHAB. The result confirms the existence of the long alkyl chains in S-TEAOH-1/2. TG and DTA analyses were performed to examine the amount of organics in S-TEAOH-1/2. The weight loss below 200 °C corresponds to the removal of physically adsorbed water, while the weight loss between 200 and 800 °C mainly corresponds to the decomposed organics in the sample. As shown in Fig. 7, S-TEAOH-1/2 has a larger weight loss below 200 °C than S-TEAOH-0. It may come from physically adsorbed water on the external surface. The weight loss at 200–800 °C is *ca.* 16.5 wt% for S-TEAOH-0, and 18.7 wt% for S-TEAOH-1/2. The additional weight loss is ascribed to the removal of the organic groups coming from the DPHAB.

The FT-IR, $^{13}C$ NMR and TG–DTA characterizations clearly show that some long-alkyl chains belonging to DPHAB are introduced in S-TEAOH-1/2. However, the $(C_2H_5O)_2P(O)$–C≡ groups are not involved in the final product according to the solid-state $^{31}P$ NMR. So, to check what happened to DPHAB during the reaction, the mother liquid of S-TEAOH-1/2 after crystallization was collected, and measured the $^{31}P$ NMR spectrum (Fig. 8). It shows a strong signal at 24 ppm due to the presence of $(HO)_2P(O)$–C≡. Another weak signal at 27 ppm is

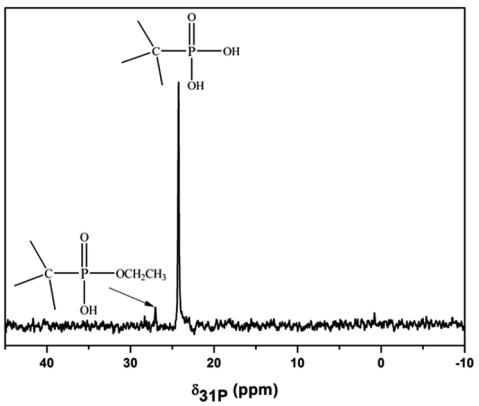


Fig. 8 $^{31}P$ NMR spectrum of mother liquid after crystallization based on sample S-TEAOH-1/2.

ascribed to the small amount of $(C_2H_5O)(HO)P(O)$–C≡.[41] $(HO)_2P(O)$–C≡ and $(C_2H_5O)(HO)P(O)$–C≡ are the hydrolysis products of $(C_2H_5O)_2P(O)$–C≡. Bases on the above analyses, it is believed that DPHAB decomposed during the reaction, and the generated $(C_2H_5O)_2P(O)$–C≡ groups or its hydrolyzed groups were inactive under the current reaction condition which stayed in the mother liquid.

In order to further understand the properties and status of organophosphorous surfactant, the molecular electrostatic potential (MEP) related to the electronic density was calculated at the optimized geometry. For comparison, the MEP of organosilane TPOAC molecule was also calculated. Fig. 9 shows the MEP maps of the two molecules. The positive (blue) regions of the maps are related to nucleophilic reactivity and the negative (red) regions to electrophilic reactivity. For both DPHAB and TPOAC, the positive (blue) regions are mainly focused on the quaternary ammonium group, and the adjacent diethoxylphosphono and methoxysilyl groups are in green color. These groups are relatively susceptible sites to interact with the anionic silicoaluminophosphate species through nucleophilic reactions. For TPOAC, methoxysilyl groups could hydrolyze and react with the silicoaluminophosphate species forming covalent bonds. The synergy between the ammonium groups and the hydrolyzed methoxysilyl groups enables the organosilane to be integrated into the SAPO product efficiently and intactly. Unlike TPOAC, there is a negative (red) region nearby the diethoxylphosphono groups due to the existence of P═O for DPHAB. This part may disturb the interaction between DPHAB and silicoaluminophosphate species. Moreover, the relatively inactivity of the hydrolyzed diethoxylphosphono groups prevents DPHAB to participate in the formation of SAPO framework. The conflicting interaction between quaternary ammonium and diethoxylphosphono groups with silicoaluminophosphate species may break up the integrity of the DPHAB molecule. As a result, the quaternary ammonium groups together with long-alkyl chains of DPHAB are involved in the SAPO product, while $(C_2H_5O)_2P(O)$–C≡ groups and its hydrolyzed products stay in the mother liquid. Nevertheless, the role of DPHAB is unique and cannot be replaced. When $N(CH_3)_3C_{16}H_{33}Br$ (CTAB) is used instead of DPHAB together with TEAOH to conduct the synthesis, pure SAPO-34 cannot be obtained (Fig. S10†).

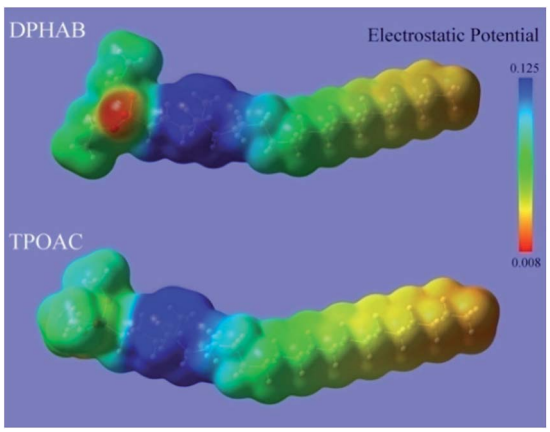


Fig. 9 Molecular electrostatic potential maps of DPHAB and TPOAC molecules.

Table 3 Lifetime[a] and product selectivity[b] of SAPO-34s in the MTO reaction (WHSV = 3 $h^{-1}$, $T$ = 450 °C)

| | | Selectivity (%) | | |
|---|---|---|---|---|
| Sample | Lifetime (min) | $C_2H_4$ | $C_3H_6$ | $C_2H_4 + C_3H_6$ |
| S-TEAOH-0 | 208 | 46.39 | 32.60 | 78.99 |
| S-TEAOH-1/9 | 292 | 45.28 | 34.72 | 80.00 |
| S-TEAOH-1/2 | 242 | 45.64 | 35.20 | 80.84 |

[a] Catalyst lifetime defined as the reaction duration with >99% methanol conversion. [b] The highest selectivity of ethylene and propylene under >99% methanol conversion.

## 4 Catalytic performances in the MTO reaction

Because of the optimized morphology of SAPO-34s synthesized with TEAOH/DPHAB, the MTO catalytic performances of S-TEAOH-1/9 and S-TEAOH-1/2 were evaluated. The results are listed in Table 3. Both samples exhibit better catalytic performance than S-TEAOH-0. The methanol conversion over 99% could be maintained for 292 and 242 min for S-TEAOH-1/9 and S-TEAOH-1/2, respectively, which are longer than that of S-TEAOH-0 (208 min). The light olefin (ethylene plus propylene) selectivity for S-TEAOH-1/9 and S-TEAOH-1/2 reach to 80.00% and 80.84%, respectively, which are higher than that of S-TEAOH-0 (78.99%). The large secondary particle size of S-TEAOH-1/2 may be responsible for the less extension of MTO catalytic lifetime. Moreover, it is noted that the selectivity for ethylene reduces a little bit, and the propylene selectivity increases comparing with that of S-TEAOH-0. The improved mass transfer ability is associated with the enhanced propylene and reduced ethylene selectivity.[42–44] In addition, the improved catalytic property should also thank to the well kept acidity. Several negative results of the mesoporous SAPO-34 synthesized by organosilane surfactant and TEAOH template have been reported.[22,45] Although the mesoporosity is introduced, the deactivation rate is still fast due to the dramatically decreased acidity after mesopore integration. In our case, $NH_3$-TPD measurement shows that the acidity of obtained samples change little after implanting mesopores, as seen in Fig. S11.† All the three samples have two similar desorption peaks at about 190 and 440 °C in the $NH_3$-TPD profiles, which indicates that the use of organophosphorous surfactant has little effect on the acidity of SAPO products.

## 5 Conclusions

By using the self-designed organophosphorous surfactant DPHAB and microporous template TEAOH, DEA and TEA, highly crystallized SAPO-34 molecular sieve with special morphologies have been hydrothermally synthesized and

 

characterized. It is found that the crystal morphology changes obviously with the addition of DPHAB and the crystals aggregate gradually with the enhanced DPHAB/$H_3PO_4$ ratio in the reactant gel. The type of microporous template also plays an important role in determining the product morphology. TEAOH having the strongest templating ability among the investigated templates shows the best cooperation with the surfactant for the formation of nanosized and mesoporous SAPO-34. Although DPHAB decomposes during the reaction, the long-alkyl chains of DPHAB can be involved in the SAPO-34 product leading to a mesoporous structure. Moreover, the use of DPHAB has little effect on the acidity of the SAPO product, which contributes to keep the original activity of the SAPO catalyst. The MTO catalytic performance is therefore effectively improved. The work is a useful exploration on the synthesis of SAPO molecular sieve by using an organophosphorous surfactant, and the combined roles of the organophosphorous surfactant and microporous template are revealed.

## Acknowledgements

We are thankful for the financial support from the National Natural Science Foundation of China (21476228 and 21101150).

## Notes and references

1 S. T. Wilson, *Stud. Surf. Sci. Catal.*, 2007, **168**, 105–135.
2 J. Liang, H. Y. Li, S. Zhao, W. G. Guo, R. H. Wang and M. L. Ying, *Appl. Catal.*, 1990, **64**, 31–40.
3 A. J. Marchi and G. F. Froment, *Appl. Catal.*, 1991, **71**, 139–152.
4 S. Wilson and P. Barger, *Microporous Mesoporous Mater.*, 1999, **29**, 117–126.
5 http://www.syn.ac.cn/english/index.php.
6 P. Tian, Y. X. Wei, M. Ye and Z. M. Liu, *ACS Catal.*, 2015, **5**, 1922–1938.
7 L. Xu, A. P. Du, Y. X. Wei, S. H. Meng, Y. L. He, Y. L. Wang, Z. X. Yu, X. Z. Zhang and Z. M. Liu, *Chin. J. Catal.*, 2008, **29**, 727–732.
8 J. Zhu, Y. Cui, Y. Wang and F. Wei, *Chem. Commun.*, 2009, 3282–3284.
9 D. Fan, P. Tian, X. Su, Y. Y. Yuan, D. H. Wang, C. Wang, M. Yang, L. Y. Wang, S. T. Xu and Z. M. Liu, *J. Mater. Chem. A*, 2013, **1**, 14206–14213.
10 G. J. Yang, Y. X. Wei, S. T. Xu, J. R. Chen, J. Z. Li, Z. M. Li, J. H. Yu and R. R. Xu, *J. Phys. Chem. C*, 2013, **117**, 8214–8222.
11 M. Yang, P. Tian, C. Wang, Y. Y. Yuan, Y. Yang, S. T. Xu, Y. L. He and Z. M. Liu, *Chem. Commun.*, 2014, **50**, 1845–1847.
12 S. Lin, J. Y. Li, R. P. Sharma, J. H. Yu and R. R. Xu, *Top. Catal.*, 2010, **53**, 1304–1310.
13 P. F. Wang, D. X. Yang, J. Hu, J. A. Xu and G. Z. Lu, *Catal. Today*, 2013, **212**, 62.e61–62.e68.
14 T. Alvaro-Munoz, E. Sastre and C. Marquez-Alvarez, *Catal. Sci. Technol.*, 2014, **4**, 4330–4339.
15 Q. M. Sun, N. Wang, G. Q. Guo and J. H. Yu, *Chem. Commun.*, 2015, **51**, 16397–16400.
16 Y. Cui, Q. Zhang, J. He, Y. Wang and F. Wei, *Particuology*, 2013, **11**, 468–474.
17 Q. M. Sun, N. Wang, D. Y. Xi, M. Yang and J. H. Yu, *Chem. Commun.*, 2014, **50**, 6502–6505.
18 F. Wang, L. Sun, C. L. Chen, Z. Chen, Z. W. Zhang, G. H. Wei and X. M. Jiang, *RSC Adv.*, 2014, **4**, 46093–46096.
19 D. Y. Xi, Q. M. Sun, J. Xu, M. Cho, H. S. Cho, S. Asahina, Y. Li, F. Deng, O. Terasaki and J. H. Yu, *J. Mater. Chem. A*, 2014, **2**, 17994–18004.
20 Q. M. Sun, N. Wang, G. Q. Guo, X. X. Chen and J. H. Yu, *J. Mater. Chem. A*, 2015, **3**, 19783–19789.
21 C. Wang, M. Yang, P. Tian, S. T. Xu, Y. Yang, D. H. Wang, Y. Y. Yuan and Z. M. Liu, *J. Mater. Chem. A*, 2015, **3**, 5608–5616.
22 L. Chen, R. W. Wang, S. Ding, B. B. Liu, H. Xia, Z. T. Zhang and S. L. Qiu, *Chem. J. Chin. Univ.*, 2010, **9**, 1693–1696.
23 X. Y. Zhang, D. X. Liu, D. D. Xu, S. Asahina, K. A. Cychosz, K. V. Agrawal, Y. Al Wahedi, A. Bhan, S. Al Hashimi, O. Terasaki, M. Thommes and M. Tsapatsis, *Science*, 2012, **336**, 1684–1687.
24 Y. Fan, H. Xiao, G. Shi, H. Y. Liu and X. J. Bao, *J. Catal.*, 2012, **285**, 251–259.
25 D. W. Lewis, C. R. A. Catlow and J. M. Thomas, *Chem. Mater.*, 1996, **8**, 1112–1118.
26 M. Elanany, B. L. Su and D. P. Vercauteren, *J. Mol. Catal. A: Chem.*, 2007, **270**, 295–301.
27 M. Sanchez, R. D. Diaz, T. Cordova, G. Gonzalez and F. Ruette, *Microporous Mesoporous Mater.*, 2015, **203**, 91–99.
28 L. Gomez-Hortiguela, J. Perez-Pariente, F. Cora, C. R. A. Catlow and T. Blasco, *J. Phys. Chem. B*, 2005, **109**, 21539–21548.
29 M. Zokaie, D. S. Wragg, A. Gronvold, T. Fuglerud, J. H. Cavka, K. P. Lillerud and O. Swang, *Microporous Mesoporous Mater.*, 2013, **165**, 1–5.
30 H. Sun, *J. Phys. Chem. B*, 1998, **102**, 7338–7364.
31 B. Y. Liu, C. Li, Y. Q. Ren, Y. Z. Tan, H. X. Xi and Y. Qian, *Chem. Eng. J.*, 2012, **210**, 96–102.
32 B. Y. Liu, Y. Z. Tan, Y. Q. Ren, C. Li, H. X. Xi and Y. Qian, *J. Mater. Chem.*, 2012, **22**, 18631–18638.
33 B. Y. Liu, F. Chen, L. M. Zheng, J. H. Ge, H. X. Xi and Y. Qian, *RSC Adv.*, 2013, **3**, 15075–15084.
34 A. Inayat, I. Knoke, E. Spiecker and W. Schwieger, *Angew. Chem., Int. Ed.*, 2012, **51**, 1962–1965.
35 H. Xue, Z. H. Li, H. Dong, L. Wu, X. X. Wang and X. Z. Fu, *Cryst. Growth Des.*, 2008, **8**, 4469–4475.
36 L. Guo, X. J. Bao, Y. Fan, G. Shi, H. Y. Liu and D. J. Bai, *J. Catal.*, 2012, **294**, 161–170.
37 K. Liu, H. P. You, G. Jia, Y. H. Zheng, Y. J. Huang, Y. H. Song, M. Yang, L. H. Zhang and H. J. Zhang, *Cryst. Growth Des.*, 2010, **10**, 790–797.
38 L. Zhang, J. Bates, D. H. Chen, H. Y. Nie and Y. N. Huang, *J. Phys. Chem. C*, 2011, **115**, 22309–22319.
39 J. Tan, Z. M. Liu, X. H. Bao, X. C. Liu, X. W. Han, C. Q. He and R. S. Zhai, *Microporous Mesoporous Mater.*, 2002, **53**, 97–108.
40 W. L. Shen, X. Li, Y. X. Wei, P. Tian, F. Deng, X. W. Han and X. H. Bao, *Microporous Mesoporous Mater.*, 2012, **158**, 19–25.

41 S. W. Yang, D. C. Doetschman, J. T. Schulte, J. B. Sarnbur, C. W. Kanyi and J. D. Fox, *Microporous Mesoporous Mater.*, 2006, **92**, 56–60.
42 C. M. Wang, Y. D. Wang, H. X. Lie, Z. K. Xie and Z. P. Liu, *J. Catal.*, 2010, **271**, 386–391.
43 Y. Y. Jin, Q. Sun, G. D. Qi, C. G. Yang, J. Xu, F. Chen, X. J. Meng, F. Deng and F. S. Xiao, *Angew. Chem., Int. Ed.*, 2013, **52**, 9172–9175.
44 Z. B. Li, J. Martinez-Triguero, P. Concepcion, J. H. Yu and A. Corma, *Phys. Chem. Chem. Phys.*, 2013, **15**, 14670–14680.
45 L. L. Wu and E. J. M. Hensen, *Catal. Today*, 2014, **235**, 160–168.